Available online at www.sciencedirect.com

SciVerse ScienceDirect

journal homepage: www.elsevier.com/locate/he

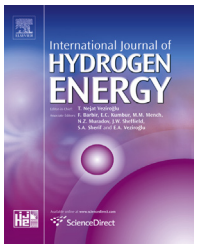

Interaction of pressure wave and propagating flame during knock

Fan Yang [a,b,*], *Huiqiang Zhang* [b], *Zheng Chen* [c,d], *Wenjun Kong* [a]

[a] *Key Laboratory of Light-duty Gas-turbine, Institute of Engineering Thermophysics, Chinese Academy of Sciences, Beijing 100190, China*

[b] *School of Aerospace, Tsinghua University, Beijing 100084, China*

[c] *SKLTCS, Department of Mechanics and Aerospace Engineering, College of Engineering, Peking University, Beijing 100871, China*

[d] *SKLTCS, Department of Aeronautics and Astronautics, College of Engineering, Peking University, Beijing 100871, China*

ARTICLE INFO

Article history:
Received 17 July 2013
Received in revised form
10 September 2013
Accepted 14 September 2013
Available online 9 October 2013

Keywords:
Knock
Spark ignition engine
Pressure wave
Propagating flame
Damköhler number

ABSTRACT

To determine the mechanism of interaction between a pressure wave and a propagating flame during knock, normal combustion and knock are numerically modeled in a simplified one-dimensional hydrogen-fueled spark ignition engine. The heat release rate of the flame front during knock abruptly increases when the pressure wave propagates through the reaction zone. The pressure wave in the diffusion zone perturbs temperature and thus causes thermal runaway at positions with low temperature and high reactant concentrations. Analysis of the Damköhler number (the ratio of gas dynamic time to chemical reaction time) and the estimated overpressure revealed that abruptly raised heat release rate during knock facilitates the amplification of the pressure wave and reinforces the interaction between pressure wave and chemical heat release.

1. Introduction

Increasing the compression ratio increases the overall efficiency of spark ignition (SI) engines. However, a high compression ratio facilitates the occurrence of unburned end-gas auto-ignition, which is the onset of knock. Knock significantly accelerates local pressure, decreases thermal efficiency, and even destroys the cylinder. Given the complexity of its chemical and physical processes, the evolution and mechanism of knock remain inadequately explained. However, using detailed chemistry numerical simulation, which can provide highly detailed and abundant information about knock process, is a potential way to investigate the evolution and mechanism of knock.

For the studies of knock, numerical simulation methods can be divided into two types. One type is based on zero-dimension combustion models using a detailed chemical mechanism, such as models by Gogan and Sundén (with detailed chemistry) [1], Noda and Kazuya (with a semi-detailed chemical mechanism) [2], and Liu and Chen (with modified Tanaka's reduced chemical kinetic model) [3]. With regard to the evolution of knock, especially after end-gas auto-

* *Corresponding author*. Key Laboratory of Light-duty Gas-turbine, Institute of Engineering Thermophysics, Chinese Academy of Sciences, Beijing 100190, China. Tel.: +86 10 8254 3043.
E-mail addresses: yanngfann@126.com, yangfan@iet.cn (F. Yang).

0360-3199/$ – see front matter
http://dx.doi.org/10.1016/j.ijhydene.2013.09.078

ignition, the interaction between the pressure wave and propagating flames in the cylinder most significantly affects the sustenance of knock. However, the zero-dimension model cannot provide any spatial information on knock evolution and on the interaction between the pressure wave and the flame.

The other type of numerical simulation methods is based on CFD (Computational Fluid Dynamics) modeling. The complex configuration like real cylinder is usually considered in such simulation. Several studies of this type are coupled with detailed chemistry [4,5], whereas most are coupled with highly reduced multi-step or single-step chemistry to avoid very large calculations [6–9]. For CFD-based numerical simulation in such configurations, the complexity of propagating flames and wave structures makes the knocking mechanism difficult to understand though the violent pressure oscillation in cylinder is obtained. Furthermore, those using simple chemistry prevent the simulation from reflecting the realistic chemical reaction effects on the evolution of knock. Therefore, due to the above intrinsic limitations, numerical studies in complex configuration still cannot fully reveal the knocking mechanism.

For the interaction between pressure wave and propagating flames which is fundamental process in knock formation and evolution, some theoretical and numerical studies [10–23] have investigated in highly simplified configurations. These studies have found important mechanisms that amplify pressure waves by auto-ignition, ranging from research on single auto-ignition centers [17,18] to that on propagating auto-ignitive reaction fronts [19–22]. The magnitude of amplified pressure waves depends on the ratio of the acoustic timescale to the excitation time for the single auto-ignition center and on the ratio of the acoustic timescale to the propagating timescale of the auto-ignitive reaction front for the successive auto-ignition mode. However, these highly simplified physical models without wall effects cannot reflect important realistic conditions for studying engine knock. Thus, we study the interaction between pressure waves and flame propagation by coupling CFD with detailed chemistry in a confined space. The most important factors for knock, such as the reflection and superposition of pressure waves, the coexistence of propagating multi-flame fronts as well as the variation of total pressure and temperature with time, are therefore considered in present study.

2. Physical model and numerical methods

The key factors for knock phenomena are SI-induced central propagating flames, walls that enable the propagation of acoustic waves in the cylinder, and end-gas auto-ignition. Based on these key factors, a simplified physical model for the knock phenomenon is proposed (Fig. 1). This model includes the initial introduced central flames, rigid walls at both ends of the computational domain, and a high-temperature, high-pressure artificial auto-ignition zone adjacent to the left wall. In this model, the propagating flame, pressure oscillation, and interaction between the flame and pressure wave are numerically simulated.

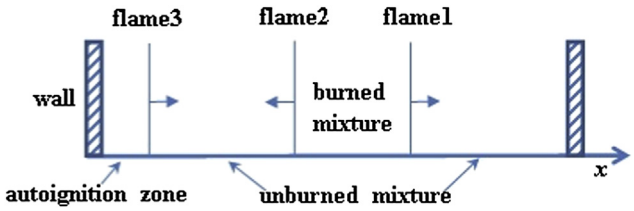

Fig. 1 – Schematic showing the physical model of knock in one-dimensional SI-engine reactor.

The knock phenomenon occurs in hydrogen-fueled internal combustion engines [24,25]. The oxidation mechanism of hydrogen is the simplest and most well developed. Therefore, we use hydrogen as the fuel in the numerical simulation. The central flames and auto-ignition zone with high temperature and pressure are set as initial conditions.

This study uses the stoichiometric mixture of hydrogen and air, an initial temperature of 750 K, and an initial pressure of 25 atm. Under these conditions, the detailed premixed planar flame structure is computed with the CHEMKIN PREMIX code [26] and then introduced to the center of the computational domain as the initial spark-ignited flame. Modeling knock assumes the occurrence of end-gas auto-ignition at the very beginning. Thus, a 1 mm-thick artificial auto-ignition zone of 2200 K and 50 atm is initially created. The total length of the computational domain is 5 cm. The homogeneous distribution of temperature and concentration of unburned gas is considered.

Based on this physical model, the one-dimensional unsteady compressible reactive flow is numerically solved using the in-house code A-SURF (Adaptive Simulation of Unsteady Reacting Flow) [27–29]. The following equations for a multi-species reactive mixture in a one-dimensional coordinate are solved in A-SURF:

$$\frac{\partial U}{\partial t}+\frac{\partial F(U)}{\partial x}=\frac{\partial F_v(U)}{\partial x}+S_R \tag{1}$$

where the vectors U, $F(U)$, $F_v(U)$, and S_R are defined as

$$U=\begin{pmatrix}\rho Y_1\\ \rho Y_2\\ \vdots\\ \rho Y_n\\ \rho u\\ E\end{pmatrix},\quad F(U)=\begin{pmatrix}\rho u Y_1\\ \rho u Y_2\\ \vdots\\ \rho u Y_n\\ \rho u^2+P\\ (E+P)u\end{pmatrix},\quad F_v(U)=\begin{pmatrix}-\rho Y_1 V_1'\\ -\rho Y_2 V_2'\\ \vdots\\ -\rho Y_n V_n'\\ \tau\\ q\end{pmatrix},$$
$$S_R=\begin{pmatrix}\omega_1\\ \omega_2\\ \vdots\\ \omega_n\\ 0\\ 0\end{pmatrix} \tag{2}$$

Here ρ is the density, u the flow velocity, and E the total energy per unit mass. The quantities, Y_k, V'_k and ω_k, are the mass fraction, diffusion velocity and production rate of species k, respectively. The production rates are specified via collection of elementary reactions using a CHEMKIN compatible database [26]. Similar to our previous study [30],

the mixture-averaged formula is employed to calculate diffusion velocity, in which the Soret diffusion of H and H_2 is considered. Moreover, a correction velocity is included to ensure the mass conservation. In the momentum equation, P is the hydrostatic pressure and $\tau=(4/3)\mu(\partial u/\partial x)$ is the viscous stress. In the energy conservation equation, the heat flux is

$$q = \lambda\frac{\partial T}{\partial x} - \rho\sum_{k=1}^{n}\left(h_k Y_k V_k'\right) \tag{3}$$

where λ is the thermal conductivity of the gas mixture and h_k is the enthalpy of species k.

To solve the conservation system in Eq. (1), the finite volume method is used and the stiff source term S_R is treated by the fractional-step procedure. In the first fractional step, the non-reactive flow is solved.

$$\left.\begin{array}{l} PDE: \dfrac{\partial U}{\partial t} + \dfrac{\partial F(U)}{\partial x} = \dfrac{\partial F_v(U)}{\partial x} \\ IC: U(x,\ t^n) = U^n \end{array}\right\} \Rightarrow \overline{U}^{n+1} \tag{4}$$

The chemistry is solved in the second fractional step for a homogeneous system

$$\left.\begin{array}{l} ODE: \dfrac{dU}{dt} = S_R(U) \\ IC: \overline{U}^{n+1} \end{array}\right\} \Rightarrow U^{n+1} \tag{5}$$

The two steps given by Eqs. (4) and (5) are denoted by operator $C^{(t)}$ and operator $S^{(t)}$, respectively. Using the Strang splitting fractional-step procedure, the solution can be evolved from its initial value U^n at time t^n, by one time step of size Δt, to a value U^{n+1} at time $t^{n+1} = t^n + \Delta t$,

$$U^{n+1} = S^{\Delta t/2}C^{\Delta t}S^{\Delta t/2}(U^n) \tag{6}$$

The Runge–Kutta, central difference, and MUSCL-Hancock schemes, all of second-order accuracy, are employed for the calculation of the temporal integration, diffusive flux, and convective flux, respectively. The CHEMKIN packages [26] are incorporated into A-SURF to calculate the temperature- and component-dependent thermodynamic and transport properties as well as the reaction rates based on the detailed chemistry of Li et al. [31]. Moreover, in order to accurately and efficiently resolve the pressure wave and propagating flame, an unstructured h-refinement (the grids in the regions of interest are locally subdivided, and some other grids may be coarsened in the regions of less importance) is employed in A-SURF. The grid refining and coarsening procedures were introduced by Sun and Takayama [32]. In our simulation, local grid addition and removal are based on the gradients of temperature and pressure. Nine grid levels (from level 0 to level 8) are utilized in this study and the finest mesh size is 1 μm (thus the largest mesh size is $1 \times 2^8 = 256$ μm). Grid convergence is tested to ensure the numerical accuracy.

3. Results and discussion

3.1. Normal combustion and knock

In normal combustion in SI engines, the spark-ignited flame propagates through the whole cylinder. The case with central laminar flames and without end-gas auto-ignition is simulated first. The introduced central laminar flames propagate into and consume the unburned mixture in both directions and finally reach the walls (Fig. 2). The pressure at $x = 3.5$ cm is recorded in the entire combustion process (Fig. 3). Pressure smoothly increases and does not oscillate.

End-gas auto-ignition is the onset of knock in SI engines. Rapid heat release with this auto-ignition significantly increases local pressure. However, the cause of knock after auto-ignition remains unknown. Therefore, to reproduce the physical state immediately after end-gas auto-ignition, we create a thin high-pressure, high-temperature zone near the left wall as the initial conditions. This case exhibits significant pressure oscillation (Fig. 3a). The filtered pressure (Fig. 3a) indicates that the maximum amplitude of pressure is about 10 atm. Knock (an abnormal combustion phenomenon) with end-gas auto-ignition is well reproduced by the proposed physical model.

Because the local pressure peak within the auto-ignition zone propagates outward and equalizes the pressure over the whole reactor, the propagating pressure wave gradually decays. After this period, the pressure wave is amplified from $t = 500$ μs to $t = 1100$ μs (Fig. 3a). During this period, intense knock is formed. Subsequently, the pressure almost never changes, indicating that the unburned mixture has been totally consumed. The lack of a flame or reaction zone implies that no acoustic actuator exists to amplify local pressure. Thus, pressure oscillation gradually decreases and then disappears. Compared with that of normal combustion, the formation and evolution of knock, especially the amplification of pressure waves, are the result of the interaction between the initial pressure wave induced by end-gas auto-ignition and the propagating flames. This observation is elaborated in the following section.

Furthermore, in SI engines, lean homogeneous operation or cooled EGR can be utilized to suppress knock by reducing the end-gas temperature [33,34]. We also plot Fig. 3b to show the influence of lean mixture ($\Phi = 0.7$) on the evolution of knock. It is seen that the initial pressure wave from auto-ignition zone is not been amplified during the whole process

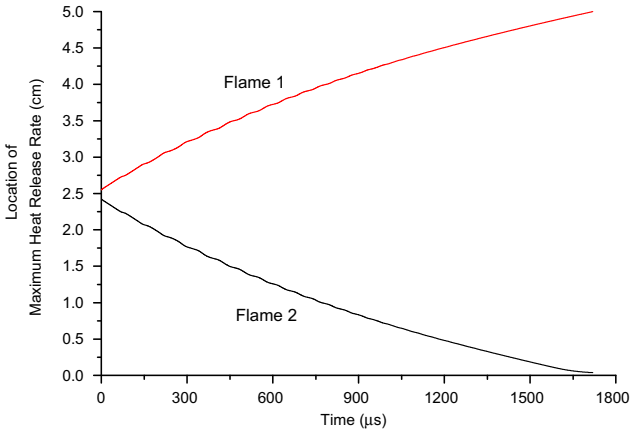

Fig. 2 – Trajectory of spark-ignited flames for normal combustion, showing that the two flame fronts propagate from center to right (flame 1) and left (flame 2) side separately.

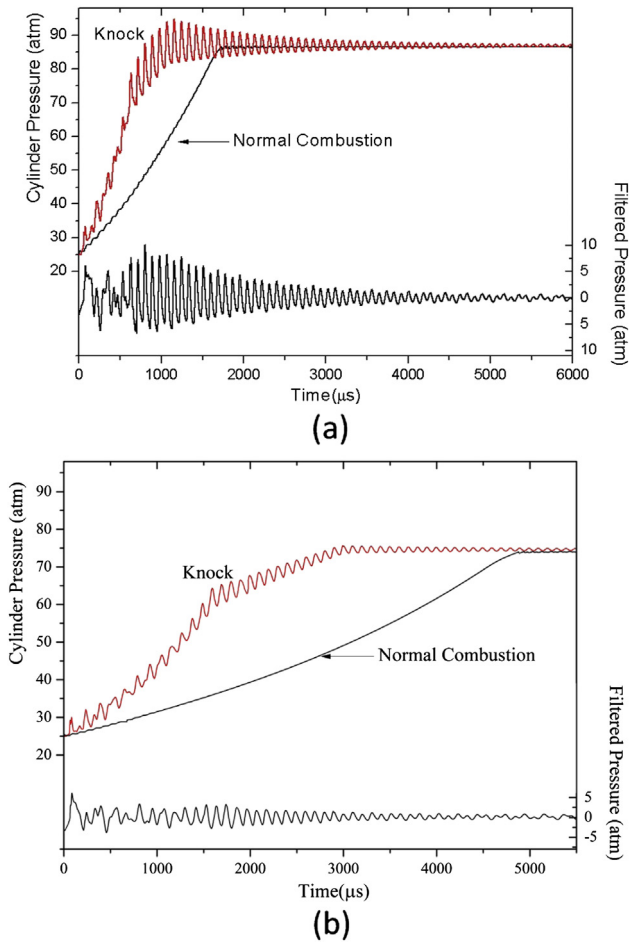

Fig. 3 – Calculated temporal variations of the cylinder pressure for normal combustion and knock, and high-passed filtered with 4 kHz cut-off frequency cylinder pressure for knock. (a) $\Phi = 1.0$ (b) $\Phi = 0.7$.

and decreases with the time, which implies that as Φ is decreased, the interaction between pressure wave and propagating flames is weak. Compared with Fig. 3a, it is apparent that the knock phenomena are more clear and representative at $\Phi = 1.0$. Thus in this paper, we choose the stoichiometric mixture for study.

3.2. *Effects of pressure wave on propagating flame*

We study normal combustion to compare it with knock. In simulation, the flame front is the position with the maximum heat release rate. The central spark-ignited flames propagate in two directions (Fig. 2). The propagation speed of flame 1 can be estimated from the trajectory. Adiabatic compression increases the temperature of the unburned gas. Consequently, the speed of flame 1 is higher than the speed of the freely propagating premixed stoichiometric H_2/air flame at 750 K and under the same pressure.

Compared with the trajectory of flame 1 in normal combustion, the propagation speed of flame 1 in abnormal mode is high. This difference is attributed to the three propagating flame fronts in abnormal combustion compared with only two such

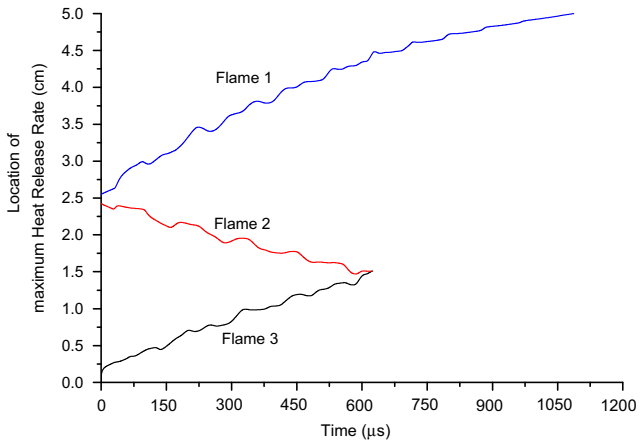

Fig. 4 – Trajectory of spark-ignited and end-gas auto-ignitive flames for knock, showing that the two spark-ignited flame fronts propagate from center to right (flame 1) and left (flame 2) side and the flame front of end-gas auto-ignition propagates from left wall to the center (flame 3).

fronts in normal combustion (Fig. 4). The pressure and temperature of the unburned gas increase more rapidly because adiabatic compression is intensified by the increased volumetric expansion of the burned gas (Figs. 3 and 5). Therefore, the third flame induced by end-gas auto-ignition accelerates compression and flame propagation. In abnormal combustion, the initial propagating pressure wave induced by end-gas auto-ignition significantly promotes the pressure and temperature oscillation of the unburned gas. This initial pressure wave and oscillation always decay before 500 μs and then abruptly rises and maintains high oscillation until the end of combustion. These phenomena are caused not by rapid compression because of the third propagating flame but by the interaction between the pressure wave and propagating flames. This interaction increases the burning rate of the flames.

To further understand this interaction, the temporal variations of the pressure and heat release rate on the flame front

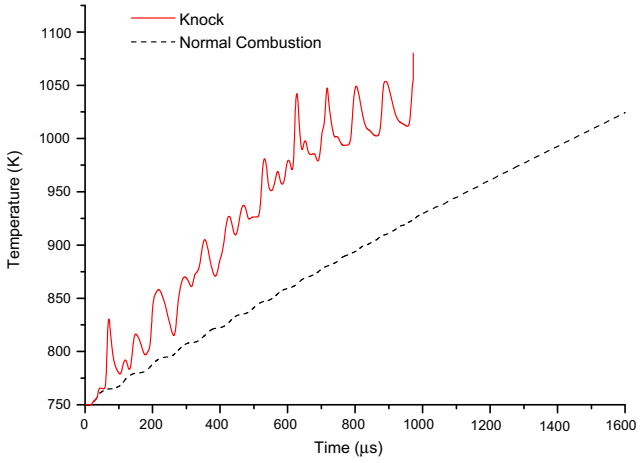

Fig. 5 – Temporal variations of unburned gas temperature at $x = 4.95$ cm next to the right wall for normal combustion and knock.

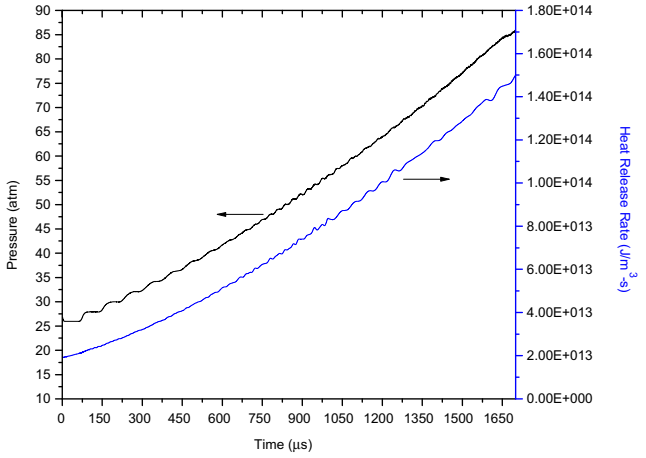

Fig. 6 – Temporal variations of pressure and heat release rate on the location of maximum heat release rate of flame 1 for normal combustion.

(defined by maximum heat release) are plotted in Figs. 6 (for normal combustion) and 7 (for knock). The heat release rate oscillates with the pressure, especially during intense knock, when this rate is sensitive to the pressure wave (Fig. 7). The chemical reaction rate is proportional to $p^n e^{-T_a/T_b}$, where n is the overall reaction order, T_a is the activation temperature, and T_b is the temperature in the reaction zone. The n of the premixed stoichiometric H_2/air flame is approximately 0.8 at elevated pressure [35]. Thus, the heat release rate at the flame front increases with increasing local pressure. For flame 1 in knock mode, when the pressure wave peak is located at the flame front at 636 μs, the heat release rate of flame 1 abruptly rises to 2.65×10^{14} J/(m^{3}s) in response to the local pressure peak (78.4 atm). In normal combustion at the same pressure (78.4 atm) and $t = 1520$ μs, the maximum heat release rate of flame 1 is 1.27×10^{14} J/(m^{3}s), lower than that in knock mode. Thus, the abrupt increase in the heat release rate of flame 1 in knock mode is not caused by the pressure effect on the chemical reaction rate.

The temporal variations of the heat release rate and temperature of flame 1 in knock mode are plotted in Fig. 8. The heat release rate does not correspond with temperature, especially after 600 μs during intense knock. Therefore, the spatial location of the maximum heat release rate of flame 1 shifts to the unburned side with lower temperature and higher reactant concentrations because of the pressure wave.

The flame structure of flame 1 in knock mode at $t = 636$ μs is shown in Fig. 9. As the reference, flame 1 in normal combustion mode at the same pressure (78.4 atm) and $t = 1520$ μs is also plotted. Based on the balance between convection and diffusion within the flame structure, laminar premixed flame thickness l_o exhibits the relation $(l_o)^2 \sim (\rho D)/w$, where w is the reaction rate evaluated at T_{ad}, ρ is the density, and D is the mass diffusivity [36]. Because ρD is pressure-insensitive, $l_o \sim w^{-1/2} \sim p^{-n/2}$, where n is 0.8. This relation implies that flame thickness decreases with increasing pressure. Because the flame structure in knock mode cannot immediately respond to the propagating pressure wave (compared with that in normal combustion at a spatially uniform pressure of

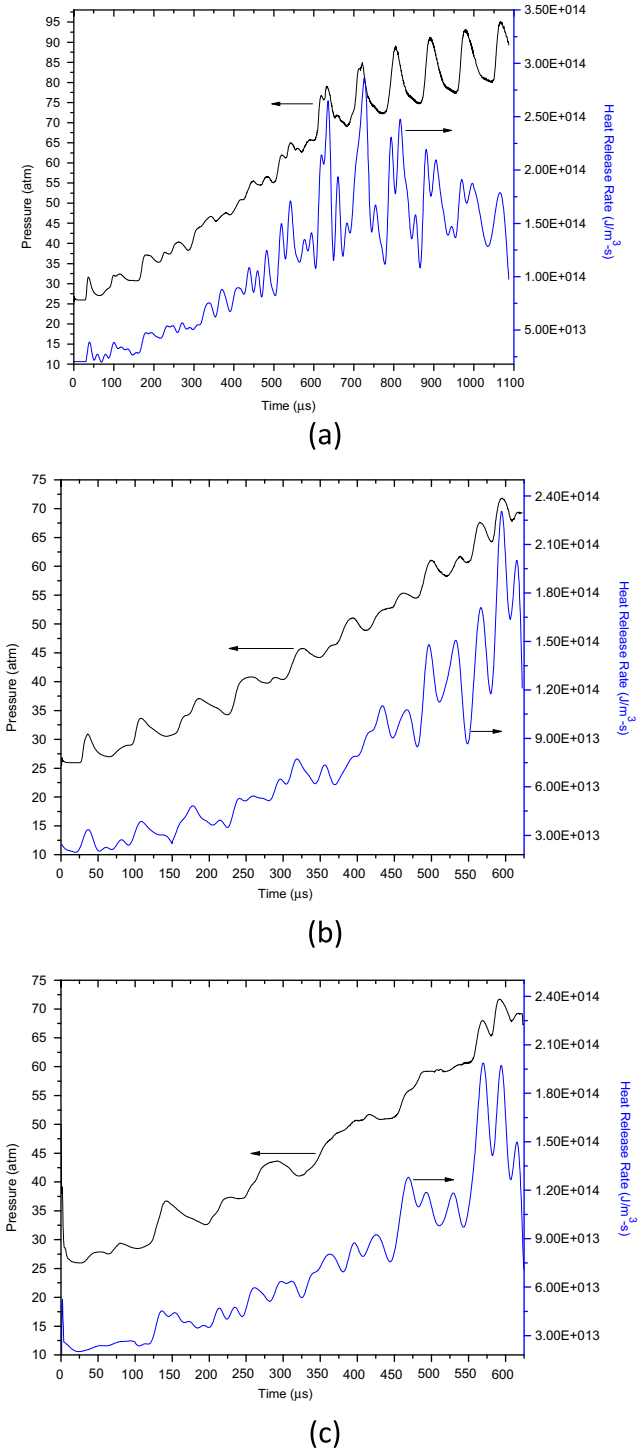

Fig. 7 – Temporal variations of pressure and heat release rate on the location of maximum heat release rate for knock. (a) Flame 1; (b) flame 2; (c) flame 3.

78.4 atm), increased local pressure only slightly influences flame thickness. Flame thickness in normal combustion is less than that in knock (Fig. 9), although the flame zone in knock mode has the same pressure (78.4 atm). The thicker flame in knock than in normal combustion causes the mass fraction of the fuel and temperature in the reaction zone of flame 1 to

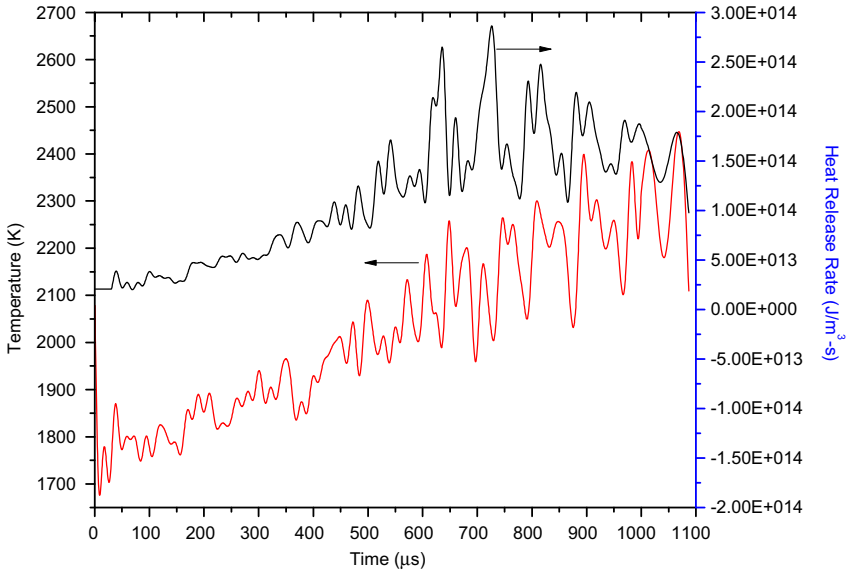

Fig. 8 – Temporal variations of temperature and heat release rate on the location of maximum heat release rate of flame 1 for knock.

have a gentler slope, implying that the chemical reaction in knock mode is weaker because of the balance between diffusion and reaction. However, the heat release rate in knock mode is higher than that in normal combustion, suggesting that combustion in knock is controlled not only by diffusion. Moreover, abruptly increasing the maximum heat release rate of flame 1 to 2.65 $\times$ 10^{14} J/(m^3s) in response to the local propagating pressure wave (Fig. 8) shifts the spatial location of this rate to the unburned side with lower temperature and higher reactant concentrations (Fig. 9). The propagating pressure wave perturbs the temperature of the unburned gas ahead of the flame front; this compressive heating by the pressure wave causes thermal runaway in the diffusion zone, where the high reactant concentrations intensify chemical reaction. Therefore, as shown in Fig. 7, the suddenly raised maximum heat release rate for flame in knock mode is due to the diffusion and pressure wave co-controlled combustion process. To further demonstrate this process, the flame 1 structures in knock mode at 10 and 195 μs are plotted in Figs. 10 and 11, respectively. As reference, the flame 1 structures in normal combustion mode are also plotted. At the very beginning of the knock mode at 10 μs, the propagating initial pressure wave

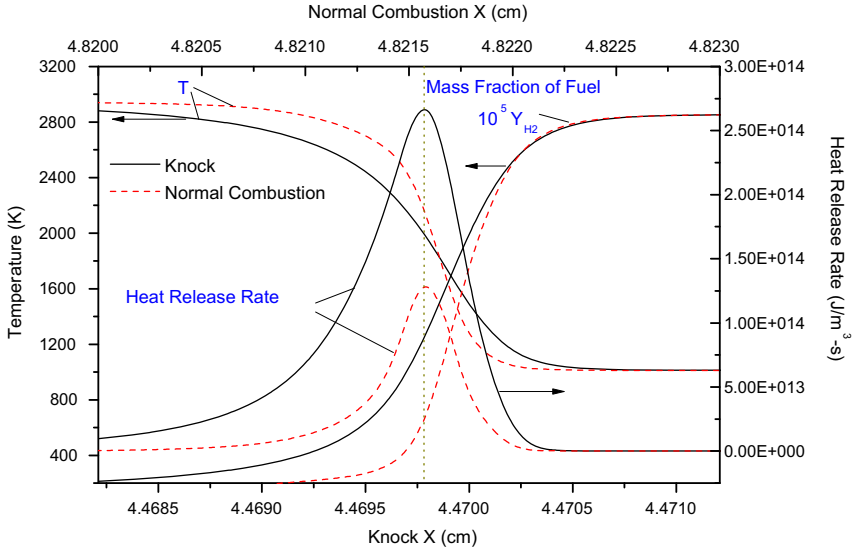

Fig. 9 – Spatial-resolved temperature, mass fraction of H_2 and heat release rate for the flame 1 in knock mode at t = 636 μs and local pressure of 78.4 atm; with the same pressure at flame front, the flame structure of flame 1 in normal combustion mode plotted for reference. Vertical dot line indicates location of the maximum heat release rate for knock and normal combustion modes.

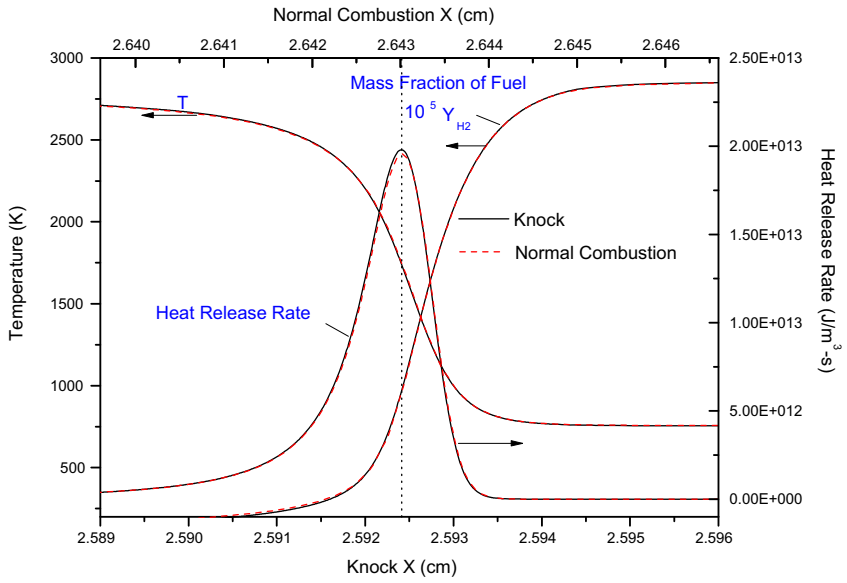

Fig. 10 – Spatial-resolved temperature, mass fraction of H_2 and heat release rate for the flame 1 in knock mode at t = 10 μs and local pressure of 25.9 atm; with the same pressure at flame front, the flame structure of flame 1 in normal combustion mode plotted for reference. Vertical dot line indicates location of the maximum heat release rate for knock and normal combustion modes.

generated by end-gas auto-ignition has not reached flame 1 and exerted no influence on it. Therefore, the combustion of flame 1 in knock mode should be the same with that in normal combustion. At the same flame front pressure, the flame 1 structure in knock mode is almost the same with that in normal combustion (Fig. 10). However, the propagating pressure wave at 195 μs exerts some influence on the combustion of flame 1 in knock mode. The flame structure in knock is similar to that in normal combustion at the same flame front pressure (Fig. 11). However, the flame zone (flame 1) in knock mode is broader than that in normal combustion, and the maximum heat release rate is higher and is found within the area with lower temperature and higher reactant concentrations. These recognized features of the flame 1 structure in knock mode at 195 μs are the same as those at 636 μs during intense knock. However, compared with the temperature

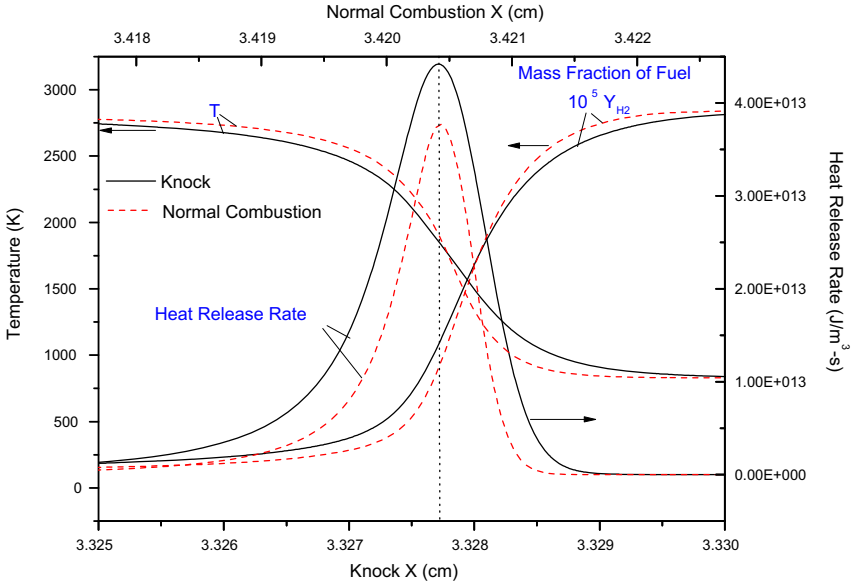

Fig. 11 – Spatial-resolved temperature, mass fraction of H_2 and heat release rate for the flame 1 in knock mode at t = 195 μs and local pressure of 36.5 atm; with the same pressure at flame front, the flame structure of flame 1 in normal combustion mode plotted for reference. Vertical dot line indicates location of the maximum heat release rate for knock and normal combustion modes.

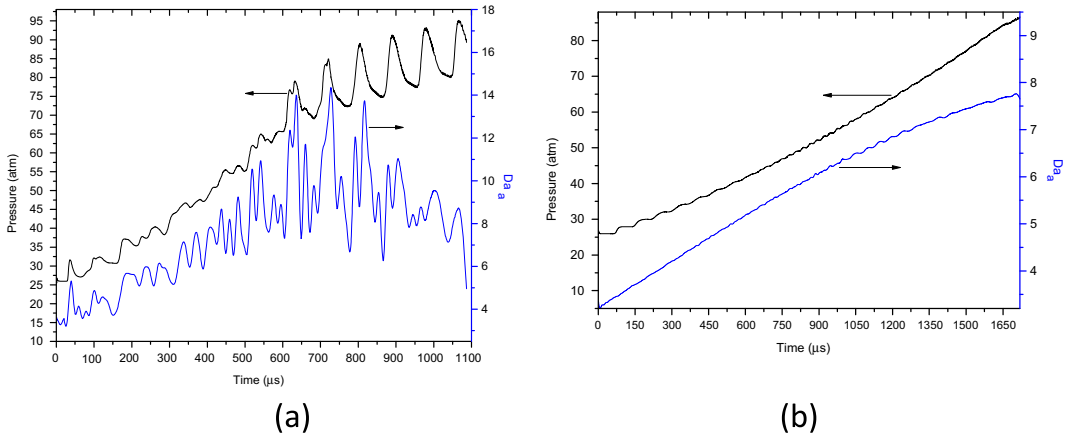

Fig. 12 – Temporal variations of pressure and Da_a on the location of maximum heat release rate of flame 1. (a) Knock; (b) normal combustion.

during this intense knock, the lower temperature of the unburned gas at 195 μs minimizes the effects of compressive heating by the pressure wave (which induces thermal runaway). Therefore, the differences in flame structure between the knock and normal combustion modes at the same flame front pressure (Fig. 11) are not significant compared with those between intense knock and normal combustion (Fig. 9).

3.3. *Amplified pressure wave during knock*

The initial local pressure peak in the auto-ignition zone propagates outward, and this propagating pressure wave gradually decreases. However, this gradually decreasing pressure wave is amplified from $t = 500$ μs to 1100 μs (Fig. 3). This phenomenon can also be observed from the temporal variation of the flame front pressure of flame 1 (Fig. 7a). Therefore, we study the mechanism for this amplification of the propagating pressure wave during knock.

Overpressure arises from the volumetric expansion of burned gas at the flame front and propagates at the speed of sound, which reduces its strength. Therefore, the magnitude of this overpressure depends on the competition between the release of chemical energy and the dynamic expansion of gas [18]. To describe the strength of this pressure wave amplification, the ratio of gas dynamic time to chemical reaction time is given by a Damköhler number:

$$Da_a = \frac{l/a}{\rho/w_F}, \tag{7}$$

where l is the total length of the reactor, a is the speed of sound, ρ is the gas density, and w_F is the mass consumption rate of fuel.

Therefore, $Da_a \to 0$ is a constant-pressure combustion process because of the infinitely fast pressure wave propagation and a reaction rate that is too low to immediately provide enough energy input to build local overpressure. At the other extreme, $Da_a \to \infty$ is a constant-volume combustion process because of the frozen propagation speed of the pressure wave and the volumetric expansion of the burned gas. At this limit, the gas in the flame zone undergoes adiabatic compression, which causes local overpressure.

We plot the temporal variation of Da_a on the location of the flame front of flame 1 in Fig. 12. During knock, the abrupt increase in the maximum heat release rate in response to the local pressure peak also rapidly increases Da_a on the flame front (Fig. 12a). This result implies that the increased intensity of chemical energy input significantly accelerates adiabatic compression and thus increases the local pressure peak. However, in normal combustion mode, although the heat release rate increases with increasing cylinder pressure, compared with this slow process of chemical energy release even at high pressure, according to the Da_a as shown in Fig. 12b, the process of gas dynamic expansion is too fast and the local gas cannot be successively compressed. Therefore, the normal combustion mode does not raise local pressure and makes the pressure spatially uniform. To further describe this mechanism of pressure wave amplification, overpressure is estimated in the following.

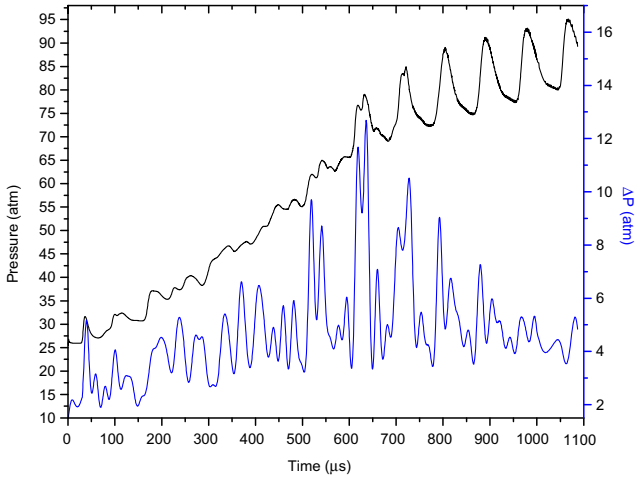

Fig. 13 – Temporal variations of pressure and ΔP on the location of maximum heat release rate of flame 1 for knock.

During knock, chemical heat is significantly released and thus overwhelms the conductive loss. Therefore, from the energy conservation perspective, the chemical energy released from the reaction zone (with heat loss disregarded) is used to heat the product mixture and perform a certain amount of expansion work. Thus,

$$q\Delta x = \Delta x \rho C_v \frac{dT}{dt} + a\Delta p, \tag{8}$$

where q is the heat release rate, Δx is the length of the reaction zone, C_v is the specific heat at constant volume, and Δp is the local overpressure. Lutz et al. [18] found that when the heat release rate rapidly rises to its maximum q_m, local temperature only slightly varies. Therefore, following Bradley [19], we disregard the accumulation term of Eq. (2). Overpressure can then be approximated by

$$\Delta p = q_m \Delta x / a. \tag{9}$$

The temporal variation of Δp on the flame front of flame 1 in knock mode is plotted in Fig. 13; the local pressure is superimposed as a reference. Abruptly increasing Da_a (Fig. 12a), makes the overpressure sensitive to the local pressure peak during knock after 500 μs. From 500 μs to 750 μs, the shape of the pressure peak is similar to that of the overpressure (Fig. 13), and Da_a increases (Fig. 12a). Therefore, the pressure on the flame front during this period is significantly amplified, and the interaction between the flame and pressure wave is further strengthened.

In SI engine, combustion always takes place within a turbulent flow field and the distribution of temperature or concentration for combustible mixture is inhomogeneous, while we limit our focus to investigate laminar combustion regimes with homogeneous unburned gas. Turbulence increases combustion speed, which could cause the flame front to pass through the unburned zone before the end-gas reaches auto-ignition condition. Thus the turbulence has positive effects on suppressing the formation of knock. Through this investigation, we can reasonably deduce that the turbulence also suppresses the evolution of knock after the occurrence of end-gas auto-ignition. This is because the higher turbulence intensity leads to a shorter burn duration, which diminishes the frequence of the interaction between propagating flame front and pressure wave, and thereby limits the amplification of the initial pressure wave from end-gas auto-ignition. By the same token, when the inhomogeneities of unburned mixture facilitate the combustion and increase the burning rate, the knock will be suppressed. The opposite holds for the negative effects of inhomogeneities on combustion. Furthermore, in practice, during knock the interactions between pressure wave and flames always occur in 3-D cylinder and their intensities vary in different directions. However, these interactions have the same basic process and mechanism, which have been studied above.

4. Conclusions

The proposed physical model of combustion in an SI hydrogen engine describes the phenomena of normal combustion and knock. To describe the mechanism of knock, the interaction between the pressure wave and propagating flame is investigated. For the evolution of knock, the initial pressure wave induced by end-gas auto-ignition plays a crucial role. This propagating initial pressure wave perturbs the temperature of the unburned gas near the flame front and thermal runaway is induced in the diffusion zone with low temperature and high reactant concentrations, thus the heat release rate of the flame increases rapidly and thereby amplifies this pressure wave. During knock as the propagating pressure wave is strengthened, the temperature perturbation of the unburned gas near the flame front further increases. Moreover, with increasing the cylinder pressure, the unburned gas temperature increases. Therefore, during knock the heat release rate at the flame front is more sensitive to the local pressure variation and the maximum heat release rate abruptly rises when the pressure wave propagates though the flame zone.

We have also studied the mechanism for the amplification of the pressure wave by the propagating flame during knock, through the analysis of a Damköhler number Da_a, which is introduced based on the ratio of the gas dynamic time to the chemical reaction time. A null Damköhler number corresponds to constant-pressure combustion, whereas an infinity value corresponds to constant-volume combustion. During knock Da_a at flame front and the estimated overpressure are higher than those in normal combustion. Thus, compared with normal case, the combustion of knock behaves more like constant-volume process, indicating that the rapidly raised heat release rate during knock can make the process of chemical energy deposition faster than the gas expansion and the local pressure wave is amplified.

Acknowledgment

This work was supported by the National Natural Science Foundation of China (under Grant Nos. 51106084, 51036004 and 50936005).

REFERENCES

[1] Gogan A, Sundén B, Montorsi L, Ahmedand S. Knock modeling: an integrated tool for detailed chemistry and engine cycle simulation. SAE 2003-01-3122; 2003.
[2] Noda T, Hasegawa K, Kubo M, Itoh T. Development of transient knock prediction technique by using a zero-dimensional knocking simulation with chemical kinetics. SAE 2004-01-0618; 2004.
[3] Liu Z, Chen R. A zero-dimensional combustion model with reduced kinetics for SI engine knocks simulation. Combust Sci Technol 2009;181:828–52.
[4] Liang L, Reitz R, Iyer C, Yi J. Modeling knock in spark-ignition engines using a G-equation combustion model incorporating detailed chemical kinetics. SAE 2007-01-0165; 2007.
[5] Omote H, Wakisaka T, Takada Y, Takai K, Nakazono T, Nishimura A. CT2-1: application of a reduced elementary reaction scheme to three-dimensional numerical simulation of knocking phenomenon in a spark ignition engine fueled by LPG-DME mixture (CT: combustion, thermal and fluid science, general session papers). In: The international symposium on diagnostics and modeling of combustion in internal combustion engines 2008. p. 491–8.

[6] Blunsdon C, Dent J. The simulation of autoignition and knock in a spark ignition engine with disk geometry. Society of Automotive Engineers; 1994.
[7] Eckert P, Kong SC, Reitze RD. Modeling autoignition and engine knock under spark ignition conditions. SAE Trans 2003;112:100–11.
[8] Kong SC, Han Z, Reitz RD. The development and application of a diesel ignition and combustion model for multidimensional engine simulation. SAE 950278; 1995.
[9] Kaario O, Larmi M, Tanner F. Comparing single-step and multi-step chemistry using the laminar and turbulent characteristic time combustion model in two diesel engines. SAE 2002-01-1749; 2002.
[10] Peters N, Ludford GSS. The effect of pressure variations on premixed flames. Combust Sci Technol 1983;34:331–44.
[11] Ledder G, Kapila AK. The response of premixed flames to pressure perturbations. Combust Sci Technol 1991;76:21–44.
[12] Van Harten A, Kapila A, Matkowsky B. Acoustic coupling of flames. SIAM J Appl Math 1984;44:982–95.
[13] Keller D, Peters N. Transient pressure effects in the evolution equation for premixed flame fronts. Theor Comp Fluid Dyn 1994;6:141–59.
[14] Mcintosh AC. Pressure disturbances of different length scales interacting with conventional flames. Combust Sci Technol 1991;75:287–309.
[15] Mcintosh AC, Wilce SA. High-frequency pressure wave interaction with premixed flames. Combust Sci Technol 1991;79:141–55.
[16] McIntosh AC. Deflagration fronts and compressibility. Philos T R Soc A 1999;357:3523–38.
[17] Meyer JW, Oppenheim AK. Dynamic-response of a plane-symmetrical exothermic reaction center. AIAA J 1972;10:1509–13.
[18] Lutz AE, Kee RJ, Miller JA, Dwyer HA, Oppenheim AK. Dynamic effects of autoignition centers for hydrogen and C1,2-hydrocarbon fuels. In: Symposium (International) on combustion. Elsevier; 1989. p. 1683–93.
[19] Bradley D. 'Hot spots' and gasoline engine knock. J Chem Soc, Faraday Trans 1996;92:2959–64.
[20] Bradley D, Morley C, Gu X, Emerson D. Amplified pressure waves during autoignition: relevance to CAI engines. SAE Trans 2002;111:2679–90.
[21] Gu XJ, Emerson DR, Bradley D. Modes of reaction front propagation from hot spots. Combust Flame 2003;133:63–74.
[22] Bradley D, Kalghatgi GT. Influence of autoignition delay time characteristics of different fuels on pressure waves and knock in reciprocating engines. Combust Flame 2009;156:2307–18.
[23] Candel S, Durox D, Ducruix S, Birbaud AL, Noiray N, Schuller T. Flame dynamics and combustion noise: progress and challenges. Int J Aeroacoust 2009;8:1–56.
[24] White CM, Steeper RR, Lutz AE. The hydrogen-fueled internal combustion engine: a technical review. Int J Hydrogen Energy 2006;31:1292–305.
[25] Verhelst S, Wallner T. Hydrogen-fueled internal combustion engines. Prog Energy Combust 2009;35:490–527.
[26] Kee RJ, Grcar JF, Smooke M, Miller J. PREMIX: a Fortran program for modeling steady laminar one-dimensional premixed flames. Sandia Report SAND85–8240; 1985.
[27] Chen Z, Burke MP, Ju YG. Effects of Lewis number and ignition energy on the determination of laminar flame speed using propagating spherical flames. Proc Combust Inst 2009;32:1253–60.
[28] Chen Z. Effects of radiation and compression on propagating spherical flames of methane/air mixtures near the lean flammability limit. Combust Flame 2010;157:2267–76.
[29] Chen Z. On the extraction of laminar flame speed and Markstein length from outwardly propagating spherical flames. Combust Flame 2011;158:291–300.
[30] Liang W, Chen Z, Yang F, Zhang H. Effects of Soret diffusion on the laminar flame speed and Markstein length of syngas/air mixtures. Proc Combust Inst 2013;34:695–702.
[31] Li J, Zhao ZW, Kazakov A, Dryer FL. An updated comprehensive kinetic model of hydrogen combustion. Int J Chem Kinet 2004;36:566–75.
[32] Sun M, Takayama K. Conservative smoothing on an adaptive quadrilateral grid. J Comput Phys 1999;150:143–80.
[33] Zhen XD, Wang Y, Xu SQ, Zhu YS, Tao CJ, Xu T, et al. The engine knock analysis – an overview. Appl Energy 2012;92:628–36.
[34] Grandin B, Angstrom H. Replacing fuel enrichment in a turbo charged SI engine: lean burn or cooled EGR. SAE 1999-01-3505; 1999.
[35] Law CK. Combustion physics. New York: Cambridge University Press; 2006.
[36] Law CK. Propagation, structure, and limit phenomena of laminar flames at elevated pressures. Combust Sci Technol 2006;178:335–60.